Dust collection after the high fluence campaign of the WEST tokamak

C. Arnas, A. Campos, M. Diez, E. Bernard, C. Brun, C. Martin, F. Gensdarmes, S. Peillon, E. Tsitrone

Nuclear Materials and Energy 42 (2025) 101848

Contents lists available at ScienceDirect

Nuclear Materials and Energy

journal homepage: www.elsevier.com/locate/nme

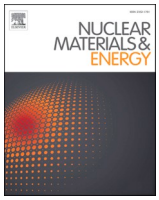

Dust collection after the high fluence campaign of the WEST tokamak☆

C. Arnas [a,*], A. Campos [b], M. Diez [c], E. Bernard [c], C. Brun [c], C. Martin [a], F. Gensdarmes [d], S. Peillon [d], E. Tsitrone [c], the WEST team[1]

[a] CNRS, Aix-Marseille Université, PIIM, 13397 Marseille, France
[b] Aix-Marseille Université , CNRS, Centrale Marseille, FSCM, CP2M, 13397 Marseille, France
[c] CEA Cadarache, IRFM, 13108 St-Paul-Lez-Durance, France
[d] LPMA, IRSN, 91192 Gif-sur-Yvette, France

ARTICLE INFO

Keywords:
WEST tokamak
Tokamak dust
Tungsten layer flaking
Tungsten nanoparticles

ABSTRACT

For Phase 2 of WEST, the lower divertor was entirely equipped with actively cooled ITER grade plasma-facing units made of chains of tungsten beveled monoblocks. In this configuration, dust particles were collected in 2023, after the first plasma campaign mainly dedicated to repetitive long pulses in the conditions of attached plasmas to the divertor. Due to a high particle fluence and a significant tungsten erosion, large quantities of dust were produced. In addition to those produced during off-normal events and the flaking of deposits which are typical of tokamak wall erosion, dust particles due to the flaking of pure tungsten thin layers deposited on the shadowed areas of beveled monoblocks were found. As specific characteristic, these thin layers may not adhere to the divertor and consequently, may be peeled off and mobilized during plasma operation.

1. Introduction

Plasma-wall interaction generates dust particles of sizes varying from a few nanometers to hundreds of microns. In tokamaks with metal divertor, they come from molten metal droplets produced during off-normal events (arcing, disruptions, runaway electrons…) identified in AUG, JET, Alcator C-Mod and WEST [1–7]. The flaking of deposited layers due to wall conditioning and sputtering also produces dust [1,2,4–7]. Recently, tungsten (W) nanoparticles of sizes as small as 5 nm were found in WEST [7].

When dust particles are produced in large quantities, they can limit the expected performances. Due to their low adhesion to plasma-facing components, they can produce hot spots during long pulses, which were correlated to asymmetric radiation of the plasma edge, leading sometimes to plasma termination [8]. The potential reinjection during early discharge stages can also impact the plasma start-up as shown in relevant ITER-like experiments and modeling [9–11] and FTU [12]. During plasma operation in JET, intense radiation spikes have been correlated to dust events [13]. In WEST, Unidentified Flying Objects (UFOs) originating mostly from deposited layers of low adhesion were divided in three classes according to how they affect the discharges [14]. Modeling have shown that even bursts of W dust could result in large perturbations of the divertor power load in ITER [15]. In addition to the effects of high-Z plasma contamination, other implications for fusion operation have been considered. Due to their large surface areas, dust particles can potentially retain tritium which could impact the fuel cycle efficiency [16,17]. Additionally, dust adds a risk of explosion which raises the question of environment contamination by tritiated and activated dust [17–19].

In this article, new highlights on the dust production during long plasma pulses and a high particle fluence in the WEST tokamak are reported. The latter is now equipped with an actively cooled ITER grade divertor where the plasma facing units consists of W beveled monoblocks in the toroidal direction [20,21]. In this context and in a regime of attached plasmas to the divertor, large quantities of dust were produced. In addition to dust due to molten materials and the flaking of deposits early observed in WEST [7], pure W thin layers formed on the shadowed areas of the beveled monoblocks have been identified. These thin layers never found before could be peeled off during plasmas. Hence, a part of them might have participated in the production of UFOs observed during the plasma campaign, some of them leading to disruptions [14,22].

☆ This article is part of a special issue entitled: 'PSI-26' published in Nuclear Materials and Energy.

* Corresponding author.
E-mail address: cecile.arnas@univ-amu.fr (C. Arnas).

[1] http://west.cea.fr/WESTteam.

https://doi.org/10.1016/j.nme.2024.101848
Received 14 June 2024; Received in revised form 14 November 2024; Accepted 11 December 2024
Available online 20 December 2024

2. Specificities of the first plasma campaign of Phase 2 of WEST

During Phase 1 of operation of WEST (2017–2021), the lower divertor divided in 12 sectors was equipped with tungsten-coated graphite tiles (inertial PFUs) and a set of ITER-like plasma facing units (PFUs) consisting of actively cooled chains of non-beveled W monoblocks (MB). For Phase 2 (2022-present), the lower divertor consists entirely of actively cooled ITER-like PFUs. Their number is 38 per sector and each of them contains 35 beveled W MBs. These MBs are characterized by a slight tilt of their surface in the toroidal direction, the focus of this shaping being to check the improvement of mechanical and heat load constraints applied to the leading edges of downstream MBs [20]. A precise, complete study of the new configuration of the divertor of WEST and, the complexity of the resulting heat load and mechanical effects, as well as their modeling are presented in ref [21].

The first plasma campaign of Phase 2 was mainly dedicated to long plasma pulses cumulated over 3 months (January-April 2023). A total of 5.5 h of discharges was reached. About 3 h of repetitive, cumulated long pulses ~60–70 s in the conditions of attached L-mode plasmas (Te ~ 25 eV) were performed with $P_{LH} = 3.8$ MW (lower hybrid heating) leading to a high cumulated fluence on the lower divertor of ~5 10^{26} D/m^2 [22] and an expected significant tungsten erosion and migration [23] leading to deposited layers [24].

3. Method of collection and analyses of dust particles

After venting the vessel and before any maintenance operation, collections are performed on the lower divertor with the vacuum technique. A small oil-free vacuum pump (ARICA 6VK – 7 m^3/h without load) is put on a safety platform set under an open port of the tokamak. It is connected to a hand-held filter holder by means of a long plastic tube. The filter holder is loaded with thin, smooth polycarbonate membranes, 10 μm thick and 47 mm diameter (Whatman cyclopore membrane, No. 7060-4704). These membranes contain calibrated holes of 0.4 μm all over the surface. For collection, the plastic nozzle of the filter holder (hole ~2 mm diameter) is put in contact with PFUs. Then, each membrane loaded with dust is transferred with a tweezer to a dedicated plastic box in the safety platform. The collection starts again elsewhere on the divertor with a new membrane.

Dust particles were collected on three sectors of the lower divertor i.e. the sector of the outer limiter, of a ICRH antenna and LH antenna. PFUs of these sectors were only exposed to the first plasma campaign of Phase 2. For each sector, one membrane was used for collection on the high field side area (HFS) and another membrane for the low field side area (LFS).

In the laboratory, two categories of dust were identified: dust dispersed inside the plastic boxes as shown Fig. 1a) (box lid at the figure top) and those adhering to the membrane (Fig. 1b). The dust samples in a given box and on the corresponding membrane, were pressed just once with the top of a sample-holder of electron microscopy (12 mm diameter) covered with a double-sided carbon adhesive tape. Fig. 1c) shows dust on the carbon tape of a sample-holder, taken in the box. Fig. 1d) shows another sample-holder with dust taken on the bottom right of the membrane. Particles of size smaller than few tens of microns remain on the membrane surface via electrostatic force (friction with the air flow of the vacuum technique), and van der Waals and capillary forces [25].

Note that during plasma campaigns of Phase 1 during which pulses were limited to a few seconds, dust particles were dispersed on the membranes making them difficult to see with the naked eye and no dust was found on the boxes [7]. These results indicate that the produced quantities and the presence of large particles in the boxes are specific to the plasma campaign described Section 2.

Shapes, sizes, compositions were investigated with a Scanning Electron Microscope (SEM – Zeiss Gemini 500) of ultra-high resolution field emission coupled to an energy dispersive X-ray spectroscopy (EDS) detector (SDD EDAX). With an incident electron beam energy of 15 kV,

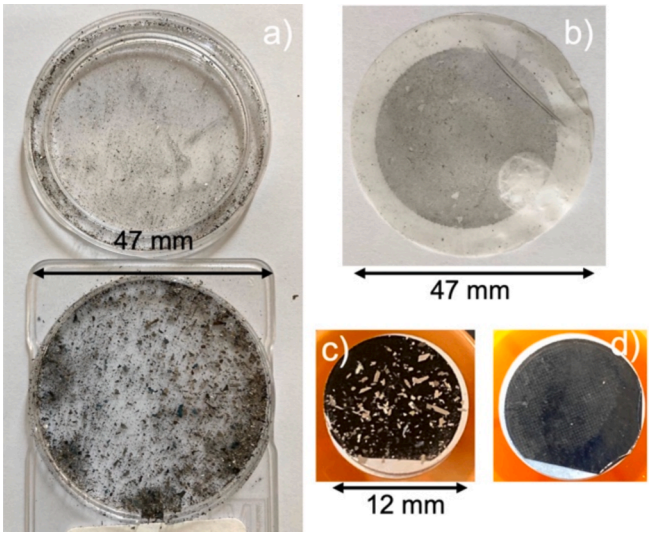

Fig. 1. Dust samples from the HFS area of the lower divertor (outer limiter sector). a) Largest dust particles dispersed inside the plastic box where the membrane shown in b) was initially placed (box lid at the top). b) Membrane with adhering dust (dark part). c) Top of a microscope sample-holder covered with carbon adhesive tape on which dust particles of the box are stuck. d) microscope sample-holder on which dust particles of the bottom right of the membrane shown in b) are stuck.

secondary electron (SE) images give the dust topography slightly below the dust surface. Backscattered electrons (BSE) are also collected (Zeiss EsB detector) to highlight different chemical compositions by means of contrast variations in a given sample or on a dust particle. In particular, this diagnostic was used to highlight the presence of nanoparticles with an incident electron beam energy of 5 kV. Moreover, in BSE images (also in SEM images of SE but not as much), heavy elements such as W appear bright and light elements such as B and C appear dark. EDS spectroscopy gives the composition details when there are mixtures of materials.

As SEM and EDS analyses have revealed similar dust characteristics for the three investigated sectors, only those of the sector of the outer limiter are presented in the following sections such as for Fig. 1).

4. Dust particles from high field side and low field side areas

4.1. Dust particles from high field side not adhering to membranes

Fig. 2a) is a SEM image of a part of dust taken in the box shown Fig. 1a), the black background being the carbon adhesive tape. This sample contains essentially small pieces of thin and thick deposited layers. Many of them have straight and sharp edges and sizes of the order of mm can be reached. In the orange circle, the dot is a dust of similar shape, of length ~40 μm measured at higher magnification. Fig. 2b) is a high magnification of the 1 mm particle shown Fig. 2a). Parallel striations of the surface are the fingerprints of machining grooves present at the MB surface on which the thin layer initially deposited. The EDS spectrum (red cross) shows that it is pure W. By tilting the sample-holder, dust particles from thin and thick layers are visible in different parts of the sample. Fig. 2c) shows an example obtained with 70° tilt.

4.2. Dust particles from high field side adhering to membranes

Fig. 3a) shows a part of dust adhering to the membrane. The magnification is the same as in Fig. 2b) for comparison. In Fig. 3b), sizes range from ~600 nm to ~15 μm and from ~80 nm to ~6 μm at higher magnification (Fig. 3c)). Fig. 3d) is a BSE image showing nanoparticles, the smallest size being ~25 nm.

The compositions of some dust found with EDS spectra (not shown

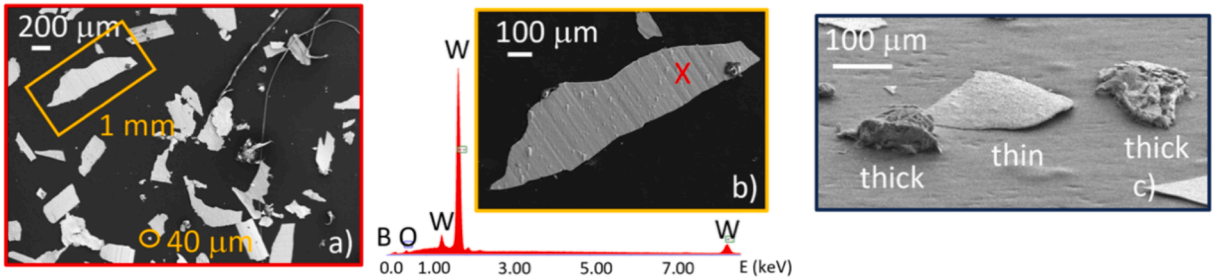

Fig. 2. A) SEM image of some largest dust particles coming from the HFS area of the lower divertor (dust in the membrane box). b) High magnification of a 1 mm dust coming from a pure W thin layer and the corresponding EDS spectrum. c) Dust particles from thin and thick layers revealed by tilting the sample-holder to 70°.

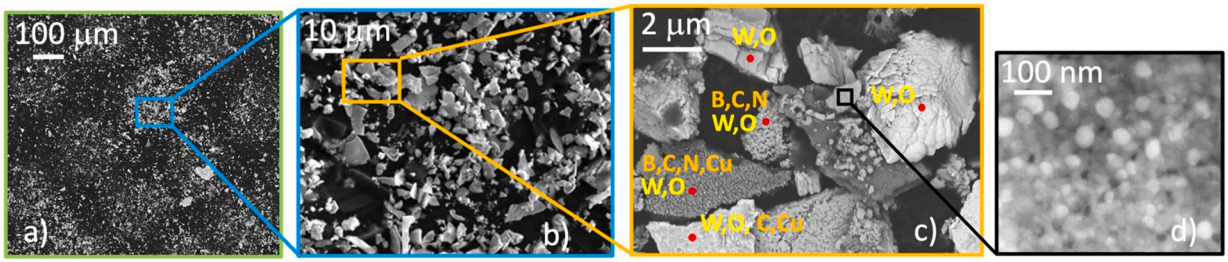

Fig. 3. A) SEM image of a part of the membrane shown Fig. 1 b). b) and c) details at higher magnifications. c) Compositions of some dust (red dots). d) BSE image showing nanoparticles. (For interpretation of the references to colour in this figure legend, the reader is referred to the web version of this article.)

here) are indicated Fig. 3c). The bright particle on the right side is W-dominated with the presence of O. All dust of same or similar brightness on this image are W-dominated while dark particles also contain light impurities. Thus, in addition to W, the surfaces of the dust particles of the left side contain impurities such as B, C and N in various proportions leading to various shades of grey. Cu traces are also present and O is present everywhere. They can have different surface porosities. W nanodroplets are seen on the surface of the central dust and W drippings on the surface of the dark particle in the bottom left. The origins are now well identified. Dust particles of complex shapes and metal mixture with irregular and rounded edges due to material melting are produced during off-normal events. This could be the origin of the right bright particle (W-dominated). Particles of sizes <1 µm deposited on the surface of the dark dust slightly to the right, have similar brightness and for a part of them, rounded edges (see at higher magnification). Dust with roughly straight and sharp edges come from the flaking of deposited layers.

4.3. Dust particles from low field side adhering to membranes

Fig. 4a) shows particles adhering initially to a membrane. They come from the same sector as Fig. 3) but from the LFS area. Less dust particles were produced/collected. The same result was observed for each investigated sector. In Fig. 4b), sizes range from ~1 µm to ~30 µm. At the right end, four EDS mappings give the chemical compositions. Dust particles on a diagonal are in W oxide (yellow and red parts, respectively). They also contain traces of N (blue part). On each side of the other diagonal, there are two particles made of pure W. On the right side of the SEM image, there are two Cu particles also oxidized.

As for the HFS area, much of the dust from the LFS samples comes from the flaking of thin and thicker deposited layers. They have the composition of materials that can be oxidized during plasma operation and also to air exposure, and may chemically associate with O when they contain C. Moreover, SEM images have revealed that dust adhering to membranes in HFS and LFS areas have multi-scale sizes ranging from several nm to several tens of microns.

5. Location of thin and thick layers producing dust particles and consequences

New results on dust produced in WEST- Phase 2 are i) the presence of large particles resulting from the flaking of thick layers and importantly, of thin layers of pure W not observed before, and ii) large produced quantities as shown Fig. 1 due to repetitive long plasma pulses.

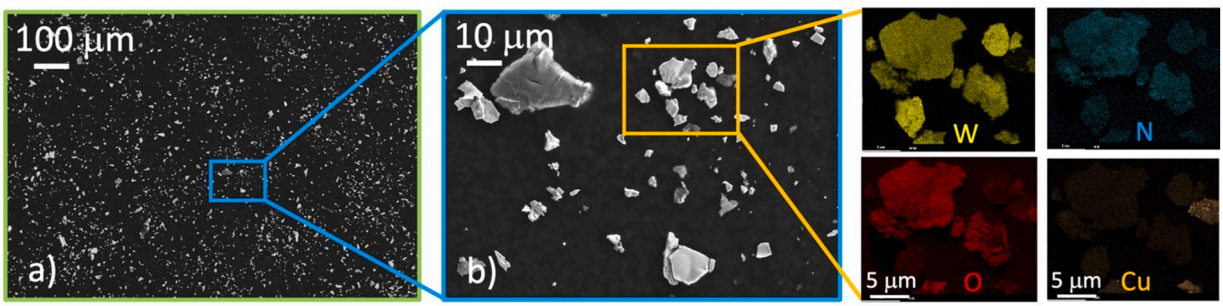

Fig. 4. A) SEM image of a part of the membrane used for collection on the LFS area of the lower divertor (outer limiter sector). Magnification of a) and b) are the same as Fig. 3a), b). On the right side, four EDS mappings give some dust compositions.

Fig. 5 shows a part of the HFS area of the lower divertor of WEST where collections were performed with a filter-holder (left side). This image shows a complex pattern of deposited layers on chains of W MBs. These deposits are located just above the upper strike point region. Dark layers on top and those located on the left and middle side of MBs are thick [26]. In particular, dark layers are easily flaked with the vacuum technique. Thin layers are on the far right. Their presence is new and explained by the fact that all MBs have a slight tilting to avoid the leading edge melting of the downstream MB during plasma operation. Pure W thin layers are then formed on the shadowed areas of the downstream MBs. The inset shows that some parts of these thin layers are already peeled off before collection. Deposits are also present on LFS areas of the lower divertor. Also there, thin layers, sometimes already peeled off before collection were formed on the shadowed parts of MBs. Moreover, it has been shown that for the repetitive long pulses of this plasma campaign, about one third of discharges ended in a disruption whose origin was UFOs. It was also established that UFO production occurred mainly from thick and thin layers of low adhesion on HFS areas and for a less extent on LFS areas [14].

6. Nanoparticles of varying sizes

Fig. 6 a) is a BSE image of a dust made of multilayers coming from a thick deposit of the HFS area. To see the internal structure on one edge (dust cross-section), the microscope holder was tilted of ~35°. Layers of various compositions are revealed through shades of grey also seen in the magnification, Fig. 6b). Unfortunately, since de dust particle was not located on the edge of the microscope holder, it was not possible to shorten the distance of the particle to the electron source after the sample was tilted and the inner layer compositions could not be obtained with a sufficiently high spatial resolution [24].

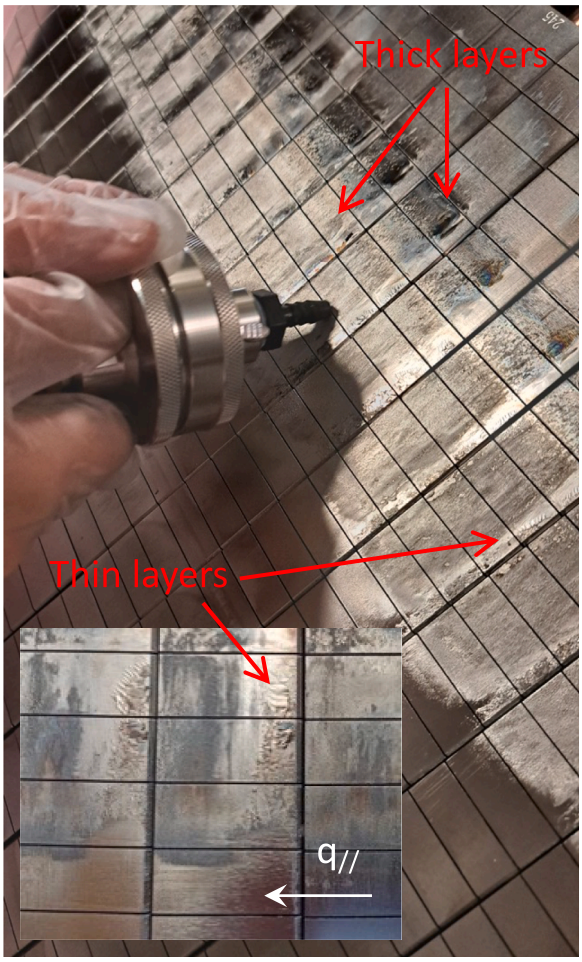

Fig. 5. Part of the HFS area of the lower divertor where collections were made (filter-holder on left side). Red arrows show thin and thick deposited layers, organized in a complex pattern. The inset shows that thin layers can be already peeled off before collection. (For interpretation of the references to colour in this figure legend, the reader is referred to the web version of this article.)

Nanoparticles (NPs) are present in different places. Those on the surface have sizes in the range 85–170 nm. A layer of NPs just below the slightly transparent upper layer (like a grey veil) are also seen in the magnification Fig. 6b) and have sizes in the range 30–65 nm. Smaller white dots of similar brightness inserted in dark parts of the cross-section are also present and shown Fig. 6b). The size estimate of these white dots is assumed to be <20 nm.

On the right side, the EDS spectrum noted 1 gives the composition of the area where NPs are present. Lines of W and O are present as well as traces of impurities such as B, C, N and Cu. As mentioned, Section 3, in BSE images and to a lesser extent in SEM images, heavy elements (W) appear bright and light elements (B, C) dark. W-dominated dust particles were already identified as bright particles Fig. 3c) and Fig. 4b). Hence, it is assumed that NPs above the thin grey layer are W-dominated. The presence of light elements in the spectrum may also give the composition of the thin grey layer due to a topography not flat at the EDS point and the presence of boronized elements around, producing EDS counts. This may be confirmed with the spectrum 2 obtained on a position of the thin layer where light element lines have raised. Moreover, it is assumed that the incident microscope electron beam of 5 keV (see Section 3) passed through this thin and light Z layer, revealing the composition of NPs just below and evidenced through W lines. It should be noted that the final internal structure of the particle of ~1 μm thickness is the result of multiple PFU erosions during multiple plasmas.

W NPs have already been observed in WEST [7,26]. They are most often separated and appear as layers on the surface of micrometer particles or as dots in cross-sections of dust made of multi-layers. They were first observed in tokamaks with graphite-based plasma facing components as TEXTOR [27,28], Tore Supra [28], JET [29] and MAST [30]. Comparisons with NPs produced in laboratory plasmas were reported and suggested a growth in the SOL region from specific successive collisions between eroded species [27,29,31,32]. With metallic PFCs, nucleation appearing by condensation of metallic vapor during cooling (nucleation in oversaturated vapor) was also proposed [33].

7. Conclusion and perspectives

The origin of shapes, sizes, compositions and produced quantities of dust depend of the conditions and duration of plasmas carried out during several months of campaign. For Phase 2 of operation of WEST, the lower divertor was entirely equipped of actively cooled ITER grade plasma facing units made of W beveled monoblocks. Dust particles were collected after the first plasma campaign of Phase 2 mainly dedicated to long repetitive pulses, in a regime of attached plasmas. In such conditions, large quantities of dust were produced. In addition to dust due to molten materials, dust particles due to the flaking of thick deposits and importantly, of thin layers of pure W not observed before were found. The latter were formed on the shadowed parts of the newly installed W beveled monoblocks. Being weakly adherent, these thin layers could be peeled-off during plasma operation and the resulting dust particles were likely involved in the production of UFOs. To complete quantitatively these results, the mass of the produced dust will be measured during the next plasma campaigns. This will provide a production dust rate and density in the conditions of an ITER-grade divertor.

CRediT authorship contribution statement

C. Arnas: Investigation. **A. Campos:** Investigation. **M. Diez:** Resources. **E. Bernard:** Resources. **C. Brun:** Investigation. **C. Martin:** Investigation. **F. Gensdarmes:** Resources. **S. Peillon:** Investigation. **E.**

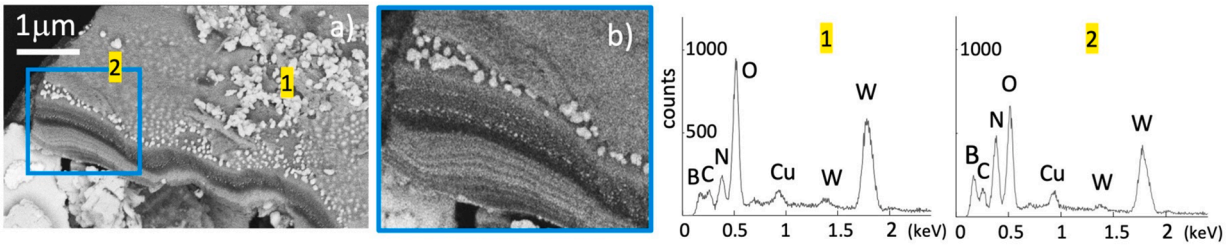

Fig. 6. A): BSE image of a dust consisting of multilayers with nanoparticles on the surface (30° tilting angle). b) Cross-section magnification showing nanoparticles below the upper thin layer; white dots inserted in dark parts are assumed to be smaller nanoparticles. EDS spectrum 1: composition mainly of nanoparticles on the surface. EDS spectrum 2: composition of the upper layer and likely of nanoparticles below, assuming the 5 kV microscope electron beam passed through this layer.

Tsitrone: Resources.

Declaration of competing interest

The authors declare that they have no known competing financial interests or personal relationships that could have appeared to influence the work reported in this paper.

Acknowledgement

This work has been carried out within the framework of the EUROfusion Consortium, funded by the European Union via the Euratom Research and Training (Grant agreement N° 101052200)- EUROfusion). Views and opinions expressed are however those of the author(s) only and do not necessary reflect those of the European Commission. Neither the European Union nor the European Commission can be held responsible for them.

Data availability

Data consist of mainly electron microscopy images or photos already shared in the paper.

References

[1] N. Endstrasser, V. Rohde, M. Balden, P. Humrickhouse, U. von Toussaint, B. J. Braams, H.-K. Chung, R. Neu, the ASDEX Upgrade team, Phys. Scr. T145 (2011) 014021.
[2] M. Balden, N. Endstrasser, P. Humrickhouse, V. Rohde, M. Rasinski, U. von Toussaint, S. Elgeti, R. Neu, the ASDEX Upgrade team, Nucl. Fusion 54 (2014) 073010.
[3] F. Brochard, V. Rohde, T. Lunt, G. Suarez Lopez, A. Shalpegin, R. Neu, ASDEX upgrade team, Nucl. Mater. Energy 18 (2019) 268.
[4] Z.A. Baron-Wiechec, E. Fortuna-Zalesna, J. Grzonka, M. Rubel, A. Widdowson, C. Ayres, J.P. Coad, C. Hardie, K. Heinola, G.F. Mattews, JET Contributors, Nucl. Fusion 55 (2015) 113033.
[5] E. Fortuna-Zalesna, J. Grzonka, M. Rubel, A. Garcia-Carrasco, A. Widdowson, A. Baron-Wiechec, L. Ciupinski, JET Contributors, Nucl. Mater. Energy 12 (2017) 582.
[6] C. Arnas, J. Irby, S. Celli, G. De Temmerman, Y. Addab, L. Couëdel, C. Grisolia, Y. Lin, C. Martin, C. Pardanaud, S. Pierson, Nucl. Mater. Energy 11 (2017) 12.
[7] C. Arnas, A. Campos, M. Diez, S. Peillon, C. Martin, K. Hassouni, A. Michau, E. Bernard, N. Fedorczak, F. Gensdarmes, C. Grisolia, B. Pégourié, E. Tsitronne, the WEST team, Nucl. Mater. Energy 36 (2023) 101471.
[8] A. Ekedahl, J. Bucalossi, V. Basiuk, S. Brémond, L. Colas, Y. Corre, E. Delchambre, D. Douai, R. Dumont, G. Dunand, G. Giruzzi, M. Goniche, S. Hong, F. Imbeaux, F. Kazarian, G. Lombard, L. Manenc, O. Meyer, L. Millon, R. Mitteau, P. Monier-Garbet, P. Moreau, B. Pégourié, F.G. Rimini, F. Saint-Laurent, F. Samaille, J. L. Schwob, E. Tsitrone, the Tore Supra Team, Nucl. Fusion 49 (2009) 095010.
[9] M. De Angeli, P. Tolias, S. Ratynskaia, D. Ripamonti, G. Riva, S. Bardin, T. Morgan, G. De Temmerman, Nucl. Mater. Energy 12 (2017) 536.
[10] S. Ratynskaia, P. Tolias, M. De Angeli, V. Weinzettl, J. Matejicek, I. Bykov, D. L. Rudakov, L. Vignitchouk, E. Thorén, G. Riva, D. Ripamonti, T. Morgan, R. Panek, G. De Temmerman, Nucl. Mater. Energy 12 (2017) 569.
[11] L. Vignitchouk, K. Paschalidis, S. Ratynskaia, P. Tolias, R.A. Pitts, Plasma Phys. Controlled Fusion 65 (2023) 015014.
[12] M. De Angeli, E. Lazzaro, P. Tolias, S. Ratynskaia, L. Vignitchouk, C. Castaldo, M. L. Apicella, G. Gervasini, G. Giacomi, E. Giovannozzi, G. Granucci, M. Iafrati, D. Iraji, G. Maddaluno, G. Riva, A. Uccello, Nucl. Fusion 59 (2019) 106033.
[13] M. Sertoli, J.C. Flanagan, M. Bacharis, O. Kardaun, A. Jarvinen, G.F. Matthews, S. Brezinsek, D. Harting, A. Cackett, E. Hodille, I.H. Coffey, E. Lazzaro, T. Pütterich, JET-EFDA Contributors, J. Nucl. Mater. 463 (2015) 837.
[14] J. Gaspar et al, "Thermal and statistical analysis of the high-Z tungsten-based UFOs observed during the first deuterium high fluence campaign of the WEST tokamak", this conference.
[15] R.D. Smirnov, S.I. Krasheninnikov, Phys. Plasmas 27 (2020) 082509.
[16] K. Ohya, A. Kirshner, Phys. Scripta 2011 (2011) 014047.
[17] S.E. Lee, Y. Hatano, M. Tokitani, S. Masuzaki, Y. Oya, T. Otsuka, N. Ashikawa, Y. Torikai, N. Asakura, H. Nakamura, K. Isobe, H. Kurotaki, D. Hamaguchi, T. Hayashi, A. Widdowson, S. Jachmich, J. Likonen, M. Rubel, JET contributors, Nucl. Mater. Energy 26 (2021) 100930.
[18] M. Shimada, R.A. Pitts, S. Ciattaglia, S. Carpentier, C.H. Choi, G. Dell Orco, T. Hirai, A. Kukushkin, S. Lisgo, J. Palmer, W. Shu, E. Veshchev, J. Nucl. Mater. 438 (2013) S996–S1000.
[19] S. Peillon, G. Dougniaux, M. Payet, E. Bernard, G. Pieters, S. Feuillastre, S. Garcia-Argote, F. Gensdarmes, C. Arnas, F. Miserque, N. Herlin-Boime, C. Grisolia, O. Pluchery, Nuc. Mater. Energy 24 (2020) 100781.
[20] M. Missirlian, M. Firdaouss, M. Richou, C. Hernandez, L. Gargiulo, J. Bucalossi, C. Brun, Y. Corre, E. Delmas, H. Greuner, B. Guillermin, J. Gunn, J.C. Hatchressian, R. Jalageas, Q. Li, M. Lipa, M. Lozano, G. Luo, C. Pocheau, H. Roche, E. Tsitrone, N. Vignal, W. Wang, A. Saille, B. Zago, the WEST Team, Fusion Eng. Des. 193 (2023) 113683.
[21] Y. Corre, M.-H. Aumeunier, A. Durif, J. Gaspar, K. Krieger, T. Loewenhoff, M. Richou, S. Ratynskaia, Q. Tichit, Y. Anquetin, R. Dejarnac, M. Diez, L. Dubus, M. Firdaouss, J. Gerardin, A. Grosjean, J.P. Gunn, T. Loarer, P. Maget, C. Martin, K. Paschalidis, E. Tsitrone, M. Wirtz, the WEST team, Nucl. Mater. Energy 37 (2023) 101546.
[22] E. Tsitrone et al, "Overview of plasma wall interactions in the first high particle fluence campaign of WEST", this conference.
[23] N. Fedorczak et al, "Tungsten gross erosion from main plasma facing components of WEST during a L-mode high fluence campaign, and its relation to the formation of divertor deposits", this conference.
[24] C. Martin et al, "Post-mortem analysis of the deposit layers on the lower divertor after the high particle fluence campaign of WEST", this conference.
[25] A. Rondeau, J. Merrison, J.J. Iversen, S. Peillon, J.-C. Sabroux, P. Lemaitre, F. Gensdarmes, E. Chassefières, Fus. Eng. Des. 98–99 (2015) 2210.
[26] C. Martin, M. Diez, A. Campos, M. Cabié, G. Giacometi, M. Balden, A. Gallo, B. Pégourié, E. Bernard, E. Tsitrone, the WEST Team, Phys. Scripta 96 (2021) 124035.
[27] J. Winter, Plasma Phys. Control. Fusion 46 (2004) B583.
[28] M. Richou, C. Martin, P. Delhae, M. Couzi, W. Saikaly, C. Brosset, B. Pégourié, A. Litnovsky, V. Philipps, P. Wienhold, J. Dentzer, C. Vix-Guterl, P. Roubin, Carbon 45 (2007) 2723.
[29] Suk-Ho Hong, A. Murari, T. Loarer, A. Huber, C. Grisolia, P. Monier-Garbet, J. Winter and JET EFDA contributors, EFDA-JET-PR(09)24, Culham Publication Services 2014.
[30] C. Arnas, C. Pardanaud, C. Martin, P. Roubin, G. De Temmerman, G. Counsell, J. Nucl. Mater. 401 (2010) 130.
[31] C. Arnas, C. Martin, P. Roubin, B. Pégourié, G. De Temmerman, K. Hassouni, A. Michau, G. Lombardi, X. Bonnin, Plasma Phys. Control. Fusion 52 (2010) 124007.
[32] G. Dinescu, C. Craciun, S.D. Stoica, C. Constantin, B.M. Mitu, T. Acsente, Molecules 29 (2024) 3539.
[33] J.P. Sharpe, B.J. Merrill, D.A. Petti, M.A. Bourham, J.G. Gilligan, J. Nucl. Mater. 290–293 (2001) 1128.